THE JOURNAL OF PHYSICAL CHEMISTRY LETTERS
A JOURNAL OF THE AMERICAN CHEMICAL SOCIETY

pubs.acs.org/JPCL

Letter

Observation and Exploitation of Spin−Orbit Excited Dipole-Bound States in Ion−Molecule Clusters

Wenjin Cao,[#] Hanhui Zhang,[#] Qinqin Yuan, Xiaoguo Zhou, Steven R. Kass,[*] and Xue-Bin Wang[*]

Cite This: *J. Phys. Chem. Lett.* 2021, 12, 11022−11028

Read Online

ACCESS | Metrics & More | Article Recommendations | Supporting Information

ABSTRACT: We report an observation of spin−orbit excited dipole-bound states (DBSs) in arginine−iodide complexes (Arg·I$^-$) by using temperature-dependent, wavelength-resolved "iodide-tagging" negative ion photoelectron spectroscopy. The observed DBSs are bound to the spin−orbit excited I($^2P_{1/2}$) level of the neutral Arg·I complex in zwitterionic conformations and identified based on the resonant enhancement due to spin−orbit electronic autodetachment from the I($^2P_{1/2}$) DBS to the I($^2P_{3/2}$) neutral ground state. The observed DBS binding energies are correlated to the dipole moments of neutral Arg·I isomers and tautomers. This work thus demonstrates a new and generic spectroscopic approach to identify ion−molecule cluster conformations based on their distinguishable dipole moments.

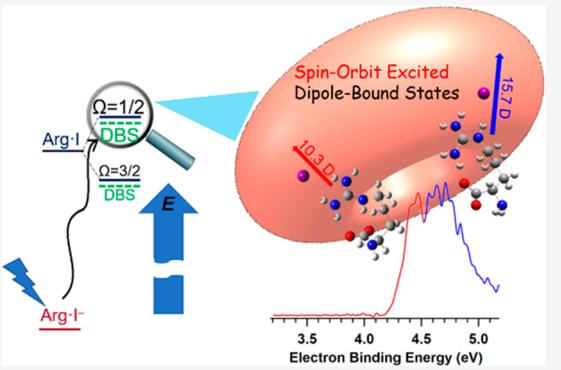

Anionic nonvalence states are ubiquitous in nature and serve as an effective "doorway" to many important electron-mediated processes including the capture of low-energy electrons,[1,2] formation of interstellar species,[3] electron-driven proton transfers,[4] as well as electron transfers in biological systems.[5−7] The excess electron in nonvalence states can be attached via Rydberg electron transfer to a polar molecule[8] or photoinduced charge-transfer from a nearby valence-bound anion.[9,10] The dipole-bound state (DBS)[11−14] with an excess electron bound to a neutral core via long-range charge−dipole interactions is most commonly observed and has been accessed via resonant photoexcitation of the corresponding valence-bound anion, where the velocity-map imaging (VMI) photoelectron spectroscopy (PES) technique is adopted to probe resonant vibrational autodetachments from the DBS.[15−18] These studies not only identified specific DBSs and concluded that the electron binding energy (EBE) of a DBS correlates with the neutral dipole moment[19] but also revealed dynamics of various processes associated with DBSs, i.e., autodetachment and internal conversion or intersystem crossing to a valence-bound state.[20−24] In principle, DBSs should also exist for anionic clusters as long as their corresponding neutral states have a sufficiently large dipole moment. Indeed, such DBSs have been observed and confirmed by Johnson and co-workers in a series of photofragmentation action spectroscopic studies on various solvated halide clusters.[25,26] Anionic clusters have long been considered as ideal model systems to mimic chemical and physical processes in bulk and at interfaces.[27] The characterization of their DBSs could serve as a scale that measures the dipole moment, which is a useful physical property in solving problems like distinguishing characteristic conformational isomers of complex ion−molecular clusters of interest, i.e., the canonical vs zwitterionic isomers of amino acids.[28]

Characterization of the DBSs of such clusters has been a challenging task. The strong intramolecular interactions in anionic clusters lead to high EBEs (often >4 eV), while the popular VMI-PES approach lacks a practical background subtraction method and suffers from a background noise issue[18] that would make it difficult to use. On the other hand, PES with a magnetic-bottle (MB) analyzer is capable of affording shot-to-shot background subtraction and is well-suited for studying high EBE species, but has a detection efficiency cutoff problem for low kinetic energy electrons.[27] As shown in Figure 1a, given the nature of the DBS, it is close lying to the neutral potential energy surface. As a result of the $\Delta\nu = -1$ propensity rule that autodetachment only occurs between adjacent vibrational levels[29] and the autodetached electrons possess extremely small electron kinetic energies, this makes them difficult to detect with a MB analyzer.

Herein, we propose a new protocol toward probing the isomer-specific DBSs of anion−molecule clusters using the arginine-iodide (Arg·I$^-$) complex as a case study, in which the spin−orbit excited DBSs are probed instead of the ground-state DBSs. We chose an amino acid-iodide complex so that we

Received: October 7, 2021
Accepted: October 28, 2021

https://doi.org/10.1021/acs.jpclett.1c03309
J. Phys. Chem. Lett. 2021, 12, 11022−11028

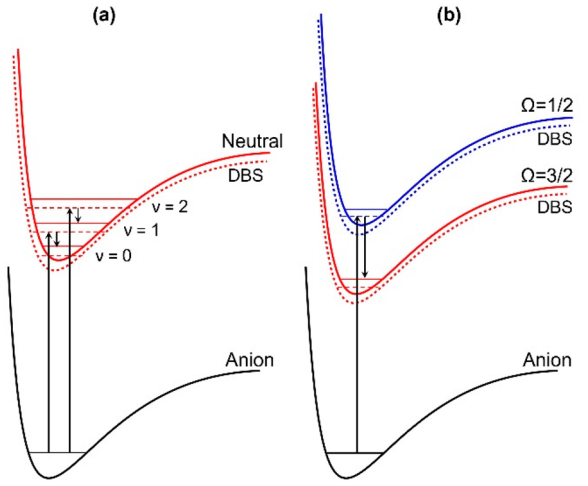

Figure 1. Schematic diagrams showing vibrational autodetachment (a) and spin−orbit autodetachment (b) from DBS resonances.

could employ the recently developed "iodide-tagging" negative ion PES technique[30,31] to interpret electronic and structural information on amino acid-iodide clusters using iodide as a messenger. This approach is based on the fact that the PE spectra of such clusters are expected to be dominated by atomic iodide transitions that exhibit two distinct bands separated by ∼0.9 eV arising from the $^2P_{3/2}$ and $^2P_{1/2}$ spin−orbit states of the iodine atom,[32−34] and different isomers can then be identified from resolved peaks based on their slightly different EBEs. The Arg·I$^-$ anion was used in this work, since arginine possesses the largest proton affinity among the α-amino acids,[35] a key aspect affecting zwitterion stability.[36] This makes arginine an ideal target to form zwitterions,[37,38] and with large dipole moments due to the charge separation, this will stabilize the DBSs formed via photoexcitation charge transfer from iodide to the arginine moiety. The existence of two spin−orbit states for iodine suggests there will be two DBSs for iodide clusters separated by ∼0.9 eV due to the spin−orbit splitting of iodine. This should lead to a brand-new autodetachment scenario—from the $^2P_{1/2}$ spin−orbit excited DBS state to the $^2P_{3/2}$ neutral state (spin−orbit electronic autodetachment, Figure 1b)—with sufficient kinetic energies for photoelectrons to be detected in the MB analyzer. Therefore, this new scheme enables DBSs of anionic clusters to be probed based on their resonance enhancement and has the capability of distinguishing different conformers with distinct dipole moments. In this Letter, we demonstrate successful characterizations on conformer-resolved spin−orbit excited DBSs of Arg·I$^-$ clusters, illustrating that the dipole moments of clusters can be spectroscopically exploited as an effective molecular descriptor to categorize distinct complex isomers.

Multiple conformers and tautomers (henceforth referred to as isomers) of the Arg·I$^-$ cluster anion were located by theoretical computations, and their coexistence in the cluster beams were confirmed by using temperature-dependent PES. Computationally, three canonical (labeled as **c1**, **c2**, and **c3**, where the letter "c" stands for canonical) and eight zwitterionic (labeled as **z1**−**z8**, with the letter "z" standing for zwitterionic) isomers were identified at the M06-2X/maug-cc-pVTZ(-PP) level of theory (Figure 2), and their CCSD(T)//M06-2X energies relative to the most stable isomer **c1** are 1.36 and 1.48 for **c2** and **c3**, and 1.24 to 2.90 kcal/mol for **z1** to **z8**, respectively (Table S1). All the Arg·I$^-$ isomers located by our calculations have two N−H···I$^-$ hydrogen bonds, but fall into two categories: **z1** and **z5**−**z8** have the iodide bound to the two terminal NH_2 groups of the guanidine, while the iodide in **c1**−**c3** and **z2**−**z4** binds to one NH_2 and the internal NH position. Dipole moments for the neutral complexes of each isomer were also computed (Figure 2 and Table S2), and the three canonical structures have an average dipole moment of 10.2 D, while the zwitterionic isomers possess larger dipole moments spanning from 10.3 to 15.7 D due to the charge separation effect. Moreover, the zwitterionic structures exhibit

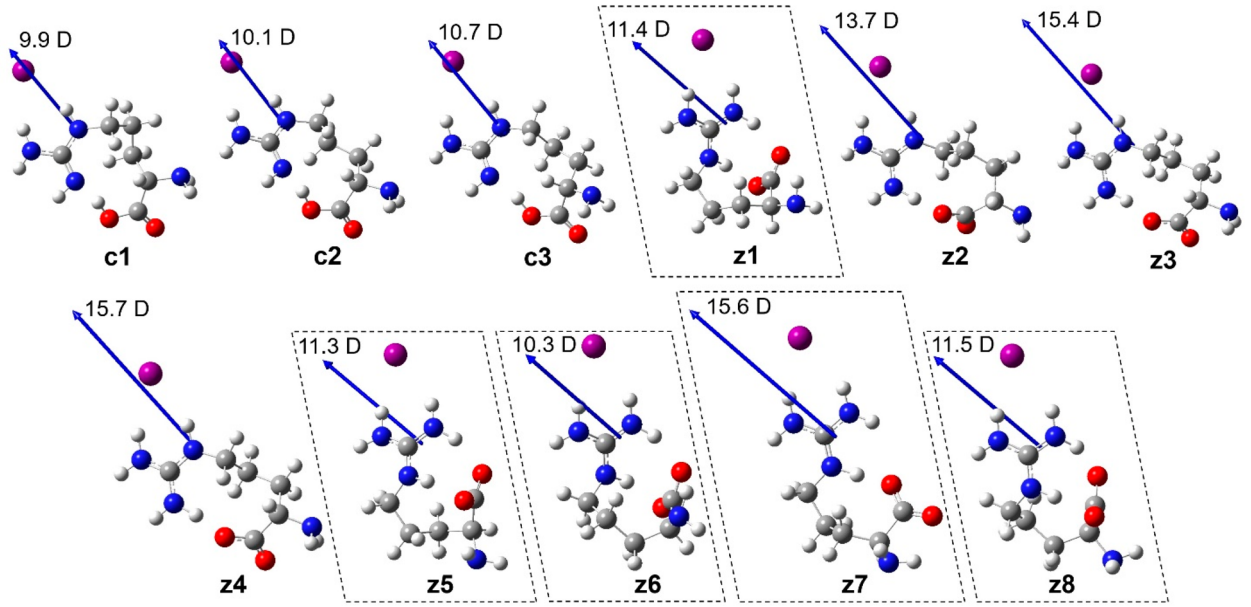

Figure 2. Calculated canonical and zwitterionic structures of the Arg·I$^-$ complex anions. The blue vectors and the numbers aside indicate the dipole moments of the corresponding neutral complexes with the anion geometries. The isomers with I$^-$ bound to two terminal NH_2 groups are boxed in with dashed lines.

https://doi.org/10.1021/acs.jpclett.1c03309
J. Phys. Chem. Lett. 2021, 12, 11022−11028

distinct dipole moments between the two categories of isomers with those that have I^- bound to two NH_2 groups generally being smaller in magnitude except for **z7**, which has a dipole moment of 15.6 D. These features lay the foundation for the characterization of these structures based upon their DBSs.

To confirm the preponderance of coexisting predicted isomers in experiments, temperature-dependent PES was first conducted. The observed 193 nm PE spectra at various temperatures from 20 to 300 K (Figure 3) show more

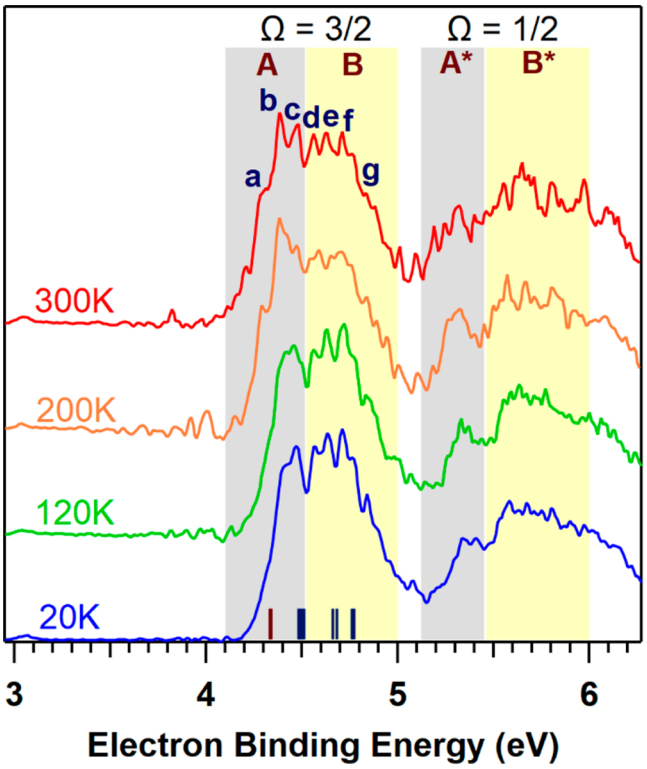

Figure 3. 193 nm PE spectra of the Arg·I^- complex obtained at various temperatures (20 K (blue), 120 K (green), 200 K (orange), and 300 K (red)). All spectra display two band systems, Ω = 3/2 and Ω = 1/2, each of which is further divided into two groups, **A** (or **A*** for Ω = 1/2) marked in light gray and **B** (or **B*** for Ω = 1/2) marked in light yellow. The calculated M06-2X VDEs of the canonical (brown) and zwitterionic (blue) isomers are represented by sticks at the bottom of the figure.

complicated spectral profiles compared to the previous "iodide-tagging" investigation of Gly·I^- and its methyl substituted derivatives.[30,31] While the spectra also exhibit two nearly identical band systems separated by ∼0.9 eV, the Ω = 3/2 and Ω = 1/2 bands, each of which consists of two groups of peaks separated by ∼0.1 eV (labeled **A** and **B** in the Ω = 3/2 band system, and **A*** and **B*** in the Ω = 1/2 one). Since none of the individual isomers solely reproduce the measured PE spectra (Figure S1), the observed bands are assigned using multiple isomers. Based on the good agreement between the calculated vertical detachment energies (VDEs) of the different structures (the brown and blue sticks in Figure 3 and Table S1) and observed peak positions in the Ω = 3/2 band system (labeled **a**−**g**), as well as the measured and simulated spectra (Figure S2), peak **a** is assigned to the three canonical isomers **c1**, **c2**, and **c3**. Peaks **b** and **c** in group **A** are assigned to isomers **z1**, **z5**, **z6**, and **z8**, while peaks **d**−**g** in group **B** are assigned to **z2**, **z3**, **z4**, and **z7** (more details on the spectral assignments can be found in the Supporting Information). Their temperature-dependent populations derived from these spectra (Figure S3) are consistent with their calculated thermochemical properties (Table S3). Since the two groups of isomers have substantial and distinguishable dipole moments and exhibit well-separated bands, the identification of isomer-specific DBSs becomes possible.

To dissect the congested spectral bands arising from various isomers of Arg·I^-, frequency-resolved PE spectra were measured at various laser wavelengths in the range of 230−250 nm (5.391−4.959 eV). Significant variations of the **A**/**B** intensity ratio, and hence the spectral appearances, were observed at different wavelengths (Figure S4), suggesting that bands **A** and **B** have distinct resonances that have been reached in the wavelength range. Figure 4 shows a typical set of the PE spectra (panel b) and resonance profiles for bands **A** and **B**, obtained by recording the total electron count rates with normalized laser output energies at different wavelengths (panel a). At a nonresonating wavelength, i.e., 193 or 250 nm, bands **A** and **B** are similar in intensity, whereas the **A**/**B** intensity ratio varies at other (resonant) wavelengths due to resonance enhancement. For example, at 238 nm **A** dominates over **B**, whereas the reverse is the case at 234 nm (Figure 4b), and a clear resonating pattern is observed with maxima at 238 nm (5.21 eV) and 234 nm (5.30 eV) for bands **A** and **B**, respectively (Figure 4a). Compared to the average VDEs of 4.44 and 4.70 eV for band systems **A** and **B**, the resonating photodetachment energies of 5.21 and 5.30 eV are more than 0.6 eV higher in energy, which is far beyond the typical range of vibronic couplings. Therefore, vibronic couplings in the Ω = 3/2 DBS of either σ-type or the recently observed π-type,[39,40] both of which have much smaller binding energies, can be excluded as the explanation for the observed resonances. The resonant photodetachment energies, on the other hand, are close to the EBE of the Ω = 1/2 band system, which exhibits maxima at approximately 5.4 and 5.6 eV for **A*** and **B***, respectively (Figure 4a).

Hereby, we assign the observed photoelectron enhancements due to autodetachment transitions from the resonances, Ω = 1/2, spin−orbit excited DBSs to the ground Ω = 3/2 neutral complex (Figure 1b). The binding energies of these DBSs can also be estimated based on the differences between the resonant photodetachment energies and EBEs of the Ω = 1/2 states to be ∼0.2 eV for the isomers in group **A** and ∼0.3 eV for those in **B**. Note that these values are estimated based on vertical transition energies, since we are unable to determine the adiabatic transition energies due to the complicated spectral profile. Nevertheless, there is a noticeable difference between the magnitude of DBS binding energies between the isomers in groups **A** and **B** with those in **B** possessing larger DBS binding energies. Based on our current assignment, **A** is mainly attributed to the mixture of **z1**/**z5**/**z6**/**z8** with an average dipole moment of 11.1 D, whereas **B** is attributed to **z2**/**z3**/**z4**/**z7** that possess an average dipole moment of 15.1 D. We suspect the binding energies for the Ω = 1/2 DBSs should be similar to those of the ground Ω = 3/2 states since the dipole moment remains largely the same for both spin−orbit states. Careful examination of the spectra indicate that there are also minor enhanced contributions from the three canonical isomers (with an average dipole moment of 10.2 D) in the vicinity of the rising edge of **A** at the resonating wavelength of 238 nm (Figure 4). It is difficult, however, to precisely record these intensity changes.

https://doi.org/10.1021/acs.jpclett.1c03309
J. Phys. Chem. Lett. 2021, 12, 11022−11028

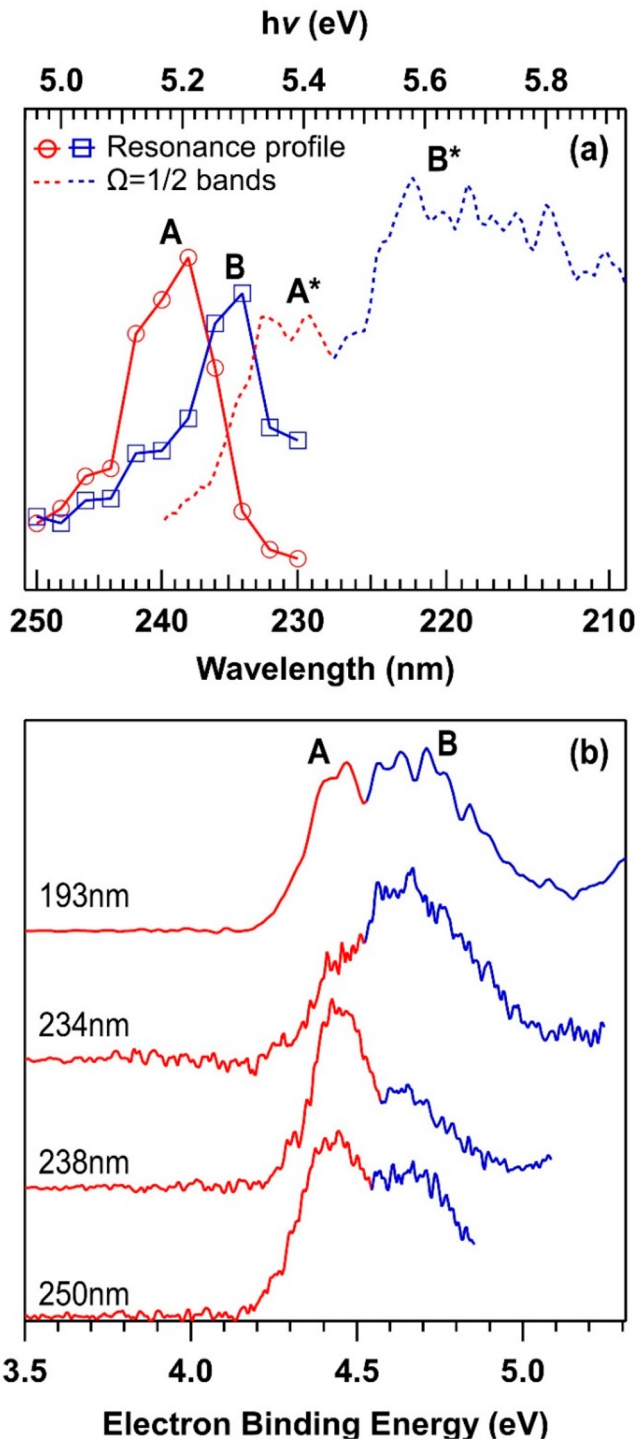

Figure 4. (a) Resonance profiles for band systems **A** (red) and **B** (blue) by recording the normalized electron count rates at each wavelength superimposed on the 20 K PE spectrum at 193 nm in the Ω = 1/2 region (red and blue dash lines for **A*** and **B***). (b) PE spectra obtained at 20 K using photodetachment wavelengths of 193, 234, 238, and 250 nm, which clearly show relative intensity changes for bands **A** and **B**.

The estimated DBS binding energies, 0.2 eV (~1600 cm^{-1}) and 0.3 eV (~2400 cm^{-1}) for isomers in groups **A** and **B**, are more than two times larger than those previously investigated in molecular DBSs,[15] a fact that is reasonably argued given the much larger dipole moments in the Arg·I complex. Furthermore, the DBS binding energy ratio is estimated to be ~1.5 (0.3 eV vs 0.2 eV) for these two groups of isomers, consistent with their calculated dipole moments (15.1 D vs 11.1 D). All these reasons support our assignments that the observed spectral pattern variation as a function of photon energy can be traced back to resonant autodetachment following photoexcitation to the excited Ω = 1/2 DBSs in the $Arg{\cdot}I^-$ complex. To the best of our knowledge, this represents the first unambiguous observation of DBSs that are bound to spin−orbit excited neutral clusters, although such type of DBS in a triatomic molecule has been discovered before.[41] The possible existence of spin−orbit excited DBSs in halide ion−molecule clusters was discussed by Johnson and co-workers. It was not observed, however, due to the Ω = 1/2 state being repulsive over the geometry of the ground state complex.[25] More excitingly, we can take advantage of these spin−orbit excited DBSs to help spectroscopically identifying different conformations in large ion−molecule clusters.

In conclusion, the isomer-specific spin−orbit excited DBSs of various zwitterionic isomers of the $Arg{\cdot}I^-$ complex have been successfully located by the resonance enhancement of the PE signal intensity in a photon energy range that is slightly below the EBE range corresponding to different anion cluster isomers. This is a result of electronic autodetachments from spin−orbit $^2P_{1/2}$ excited DBSs to the corresponding $^2P_{3/2}$ neutral ground states. The DBS binding energies are found to correlate with the magnitude of the neutral complexes dipole moments, a result that enables dipole moments as an important order parameter that has not been exploited to date to distinguish different isomers including zwitterionic conformations in the ion spectroscopy of complex anion−molecular clusters. This work demonstrates a proof-of-concept that conventional MB-PES, when coupled with a tunable UV−vis laser, turns out to be a new and effective approach to probe and tackle complex isomeric issues of ion−molecular clusters that usually have high electron detachment energies by exploiting the spin−orbit excited DBSs. This discovery of a generic spectroscopic tool will be useful for future biophysical and chemical physics research that involves ion−molecule interactions. Furthermore, competitions of electronic autodetachment against other possible channels, i.e., vibrational autodetachment and internal conversion to a different nonvalence or valence-bound state, remains a fascinating question that warrants future studies.

EXPERIMENTAL METHODS

The PE spectra in this work were obtained using a MB photoelectron spectrometer, combined with an electrospray ionization (ESI) source and a temperature-controlled cryogenic ion trap, as described elsewhere.[42] Multiple isomers of the $Arg{\cdot}I^-$ cluster were generated from solution via electrospraying an ~0.1 mM mixture of both KI and arginine (1:1 ratio) dissolved in acetonitrile/water (3:1 v/v ratio). The generated anions were transported by a radiofrequency quadruple ion guide and first detected by a quadruple mass spectrometer to optimize ESI conditions to ensure a stable and intense cluster beam. The anions were then directed by a 90° bender into the cryogenic 3D ion trap set at desired temperatures (usually 20 K, unless otherwise mentioned), where they were accumulated and cooled by collisions with cold buffer gas (20% H_2 balanced in He) for 20−100 ms. During this process, multiple isomers of $Arg{\cdot}I^-$ were kinetically isolated and retained, before being pulsed out into the extraction zone of the TOF mass spectrometer for mass

https://doi.org/10.1021/acs.jpclett.1c03309
J. Phys. Chem. Lett. 2021, 12, 11022−11028

analysis. The anions of interest were mass-selected and decelerated before being photodetached by a probe laser beam in the interaction zone of the magnetic-bottle photoelectron analyzer. Either a 193 nm (6.424 eV, GAM EX100F ArF) excimer laser or a Nd:YAG laser (Spectra-Physics Quanta-Ray Pro 270) pumped tunable OPO/OPA laser (230−250 nm or 5.391−4.959 eV, Spectra-Physics PrimoScan ULD500) beam was used for photodetachment, and operated at a 20 Hz repetition rate with the anion beam off on alternating laser shots to afford shot-by-shot background subtraction. The photoelectrons were collected at nearly 100% efficiency by the magnetic-bottle and analyzed in a 5.2-m-long electron flight tube. The recorded flight times were converted into calibrated kinetic energies using the known spectrum of $I^-/Cu(CN)_2^-$.[43−45] EBEs were subsequently obtained by subtracting the electron kinetic energies from the detachment photon energies with an electron energy resolution ($\Delta E/E$) of about 2%, i.e., ∼20 meV for 1 eV kinetic energy electrons. Intensity ratios of different isomers in each spectrum were obtained from the integrated signal counts over a certain EBE range and then normalized for the laser pulse energy and total number of scans.

COMPUTATIONAL DETAILS

Numerous initial structures for the Arg·I^- cluster anions in zwitterionic and canonical forms were systematically examined with molecular dynamics searches using semiempirical methods (AM1[46] and PM3[47]) with the Spartan software.[48] All conformations within 10 kcal mol^{-1} of the most stable one were used as initial structures for subsequent optimizations. Further geometry optimizations and harmonic frequency analyses of all candidate anions and corresponding neutral radicals were performed with DFT using the M06-2X functional[49] with Grimme's GD3 dispersion corrections,[50] which was benchmarked as a good choice for molecular systems with ionic hydrogen-bonding interactions.[28] No symmetry constraints were used in the initial optimizations, whereas appropriate point groups were used in subsequent optimizations and frequency analyses. These calculations were performed with the maug-cc-pVTZ[51,52] (and maug-cc-pVTZ-PP for I[53]) basis sets obtained from the EMSL basis set exchange.[54] Furthermore, CCSD(T)[55,56] single-point-energy calculations were carried out with the same basis set to refine the relative energies of all cluster anion isomers. Unfortunately, the CCSD(T) calculations for the open-shell neutral radicals were too computationally demanding and exceeded our resources. Therefore, the neutral dipole moment and vertical detachment energy (VDE) of each isomer was refined using the domain based local pair natural orbital coupled cluster method [DLPNO−CCSD(T)],[57] and the experimental values were compared to both the M06-2X and DLPNO−CCSD(T) results. The latter calculations were also carried out with maug-cc-pVTZ(-PP) basis sets and the corresponding auxiliary basis sets.[58] All of the DFT calculations were carried out using the Gaussian 16 software package[59] whereas the CCSD(T) and DLPNO−CCSD(T) computations were done with Molpro 2019.2[60] and ORCA 4.1.2,[61] respectively. Additionally, the Franck−Condon factors (FCFs) for spectral simulations including Duschinsky rotations were computed with the ezSpectrum program.[62] The resulting simulated stick spectra were also convoluted using the experimental line width (70 meV) and a Gaussian line shape to facilitate comparison with the measured spectra.

ASSOCIATED CONTENT

Supporting Information

The Supporting Information is available free of charge at https://pubs.acs.org/doi/10.1021/acs.jpclett.1c03309.

More details on computed isomers; More details on spectral assignments; Wavelength-dependent PE spectra to produce the resonance profile (PDF)

AUTHOR INFORMATION

Corresponding Authors

Xue-Bin Wang − *Physical Sciences Division, Pacific Northwest National Laboratory, Richland, Washington 99352, United States;* orcid.org/0000-0001-8326-1780; Email: xuebin.wang@pnnl.gov

Steven R. Kass − *Department of Chemistry, University of Minnesota, Minneapolis, Minnesota 55455, United States;* orcid.org/0000-0001-7007-9322; Email: kass@umn.edu

Authors

Wenjin Cao − *Physical Sciences Division, Pacific Northwest National Laboratory, Richland, Washington 99352, United States;* orcid.org/0000-0002-2852-4047

Hanhui Zhang − *Physical Sciences Division, Pacific Northwest National Laboratory, Richland, Washington 99352, United States; Hefei National Laboratory for Physical Sciences at the Microscale, Department of Chemical Physics, University of Science and Technology of China, Hefei, Anhui 230026, P.R. China*

Qinqin Yuan − *Physical Sciences Division, Pacific Northwest National Laboratory, Richland, Washington 99352, United States;* orcid.org/0000-0001-5771-6147

Xiaoguo Zhou − *Hefei National Laboratory for Physical Sciences at the Microscale, Department of Chemical Physics, University of Science and Technology of China, Hefei, Anhui 230026, P.R. China;* orcid.org/0000-0002-0264-0146

Complete contact information is available at: https://pubs.acs.org/10.1021/acs.jpclett.1c03309

Author Contributions

#W.C. and H.Z. contributed equally to this work.

Notes

The authors declare no competing financial interest.

ACKNOWLEDGMENTS

The work was supported by U.S. Department of Energy (DOE), Office of Basic Energy Sciences, Division of Chemical Sciences, Geosciences, and Biosciences, and performed using EMSL, a national scientific user facility sponsored by DOE's Office of Biological and Environmental Research and located at Pacific Northwest National Laboratory, which is operated by Battelle Memorial Institute for the DOE. The theoretical calculations were conducted on the EMSL Cascade Supercomputer and at the University of Minnesota Supercomputing Institute. S.R.K. acknowledges support from the National Science Foundation (CHE-1955186). X.Z. appreciates the financial support of the National Natural Science Foundation of China (No. 21873089).

REFERENCES

(1) Weber, J. M.; Ruf, M. W.; Hotop, H. Rydberg Electron Transfer to C_{60} and C_{70}. *Z. Phys. D: At., Mol. Clusters* **1996**, *37*, 351−357.

(2) Voora, V. K.; Jordan, K. D. Nonvalence Correlation-Bound Anion State of C_6F_6: Doorway to Low-Energy Electron Capture. *J. Phys. Chem. A* **2014**, *118*, 7201−7205.
(3) Fortenberry, R. C.; Crawford, T. D. Theoretical Prediction of New Dipole-Bound Singlet States for Anions of Interstellar Interest. *J. Chem. Phys.* **2011**, *134*, 154304.
(4) Eustis, S. N.; Radisic, D.; Bowen, K. H.; Bachorz, R. A.; Haranczyk, M.; Schenter, G. K.; Gutowski, M. Electron-Driven Acid-Base Chemistry: Proton Transfer from Hydrogen Chloride to Ammonia. *Science* **2008**, *319*, 936−939.
(5) Burrow, P. D.; Gallup, G. A.; Scheer, A. M.; Denifl, S.; Ptasinska, S.; Märk, T.; Scheier, P. Vibrational Feshbach Resonances in Uracil and Thymine. *J. Chem. Phys.* **2006**, *124*, 124310.
(6) Kunin, A.; Neumark, D. M. Time-Resolved Radiation Chemistry: Femtosecond Photoelectron Spectroscopy of Electron Attachment and Photodissociation Dynamics in Iodide−Nucleobase Clusters. *Phys. Chem. Chem. Phys.* **2019**, *21*, 7239−7255.
(7) Cercola, R.; Matthews, E.; Dessent, C. E. H. Near-Threshold Electron Transfer in Anion-Nucleobase Clusters: Does the Identity of the Anion Matter? *Mol. Phys.* **2019**, *117*, 3001−3010.
(8) Ciborowski, S. M.; Liu, G.; Graham, J. D.; Buytendyk, A. M.; Bowen, K. H. Dipole-Bound Anions: Formed by Rydberg Electron Transfer (RET) and Studied by Velocity Map Imaging−Anion Photoelectron Spectroscopy (VMI−aPES). *Eur. Phys. J. D* **2018**, *72*, 139.
(9) Rogers, J. P.; Anstöter, C. S.; Verlet, J. R. R. Ultrafast Dynamics of Low-Energy Electron Attachment via a Non-Valence Correlation-Bound State. *Nat. Chem.* **2018**, *10*, 341−346.
(10) Rogers, J. P.; Anstöter, C. S.; Bull, J. N.; Curchod, B. F. E.; Verlet, J. R. R. Photoelectron Spectroscopy of the Hexafluorobenzene Cluster Anions: $(C_6F_6)_n^-$ (n = 1−5) and $I^-(C_6F_6)$. *J. Phys. Chem. A* **2019**, *123*, 1602−1612.
(11) Fermi, E.; Teller, E. The Capture of Negative Mesotrons in Matter. *Phys. Rev.* **1947**, *72*, 399−408.
(12) Lykke, K. R.; Mead, R. D.; Lineberger, W. C. Observation of Dipole-Bound States of Negative Ions. *Phys. Rev. Lett.* **1984**, *52*, 2221−2224.
(13) Jordan, K. D.; Wang, F. Theory of Dipole-Bound Anions. *Annu. Rev. Phys. Chem.* **2003**, *54*, 367−396.
(14) Simons, J. Molecular Anions. *J. Phys. Chem. A* **2008**, *112*, 6401−6511.
(15) Zhu, G.-Z.; Wang, L.-S. High-Resolution Photoelectron Imaging and Resonant Photoelectron Spectroscopy via Noncovalently Bound Excited States of Cryogenically Cooled Anions. *Chem. Sci.* **2019**, *10*, 9409−9423.
(16) Lu, Y.; Tang, R.; Fu, X.; Liu, H.; Ning, C. Dipole-Bound and Valence Excited States of AuF Anions via Resonant Photoelectron Spectroscopy. *J. Chem. Phys.* **2021**, *154*, 074303.
(17) Verlet, J. R. R.; Anstöter, C. S.; Bull, J. N.; Rogers, J. P. Role of Nonvalence States in the Ultrafast Dynamics of Isolated Anions. *J. Phys. Chem. A* **2020**, *124*, 3507−3519.
(18) Weichman, M. L.; Neumark, D. M. Slow Photoelectron Velocity-Map Imaging of Cryogenically Cooled Anions. *Annu. Rev. Phys. Chem.* **2018**, *69*, 101−124.
(19) Qian, C.-H.; Zhu, G.-Z.; Wang, L.-S. Probing the Critical Dipole Moment To Support Excited Dipole-Bound States in Valence-Bound Anions. *J. Phys. Chem. Lett.* **2019**, *10*, 6472−6477.
(20) Bull, J. N.; Anstöter, C. S.; Verlet, J. R. R. Ultrafast Valence to Non-Valence Excited State Dynamics in a Common Anionic Chromophore. *Nat. Commun.* **2019**, *10*, 5820.
(21) Anstoter, C. S.; Mensa-Bonsu, G.; Nag, P.; Rankovic, M.; Kumar T. P., R.; Boichenko, A. N.; Bochenkova, A. V.; Fedor, J.; Verlet, J. R. R. Mode -SpecificVibrational Autodetachment Following Excitation of Electronic Resonances by Electrons and Photons. *Phys. Rev. Lett.* **2020**, *124*, 203401.
(22) Kang, D. H.; An, S.; Kim, S. K. Real-Time Autodetachment Dynamics of Vibrational Feshbach Resonances in a Dipole-Bound State. *Phys. Rev. Lett.* **2020**, *125*, 093001.
(23) Kang, D. H.; Kim, J.; Kim, S. K. Recapture of the Nonvalence Excess Electron into the Excited Valence Orbital Leads to the Chemical Bond Cleavage in the Anion. *J. Phys. Chem. Lett.* **2021**, *12*, 6383−6388.
(24) Yandell, M. A.; King, S. B.; Neumark, D. M. Decay Dynamics of Nascent Acetonitrile and Nitromethane Dipole-Bound Anions Produced by Intracluster Charge-Transfer. *J. Chem. Phys.* **2014**, *140*, 184317.
(25) Dessent, C. E. H.; Kim, J.; Johnson, M. A. Photochemistry of Halide Ion−Molecule Clusters:Dipole -BoundExcited States and the Case for Asymmetric Solvation. *Acc. Chem. Res.* **1998**, *31*, 527−534.
(26) Dessent, C. E. H.; Kim, J.; Johnson, M. A. Spectroscopic Observation of Vibrational Feshbach Resonances in Near-Threshold Photoexcitation of $X^-{\cdot}CH_3NO_2$ (X^-=I^- and Br^-). *Faraday Discuss.* **2000**, *115*, 395−406.
(27) Wang, X.-B. Cluster Model Studies of Anion and Molecular Specificities via Electrospray Ionization Photoelectron Spectroscopy. *J. Phys. Chem. A* **2017**, *121*, 1389−1401.
(28) Walker, M.; Harvey, A. J. A.; Sen, A.; Dessent, C. E. H. Performance of M06, M06-2X, and M06-HF Density Functionals for Conformationally Flexible Anionic Clusters: M06 Functionals Perform Better than B3LYP for a Model System with Dispersion and Ionic Hydrogen-Bonding Interactions. *J. Phys. Chem. A* **2013**, *117*, 12590−12600.
(29) Simons, J. Propensity Rules for Vibration-Induced Electron Detachment of Anions. *J. Am. Chem. Soc.* **1981**, *103*, 3971−3976.
(30) Zhang, H.; Cao, W.; Yuan, Q.; Zhou, X.; Valiev, M.; Kass, S. R.; Wang, X.-B. Cryogenic "Iodide-Tagging" Photoelectron Spectroscopy: A Sensitive Probe for Specific Binding Sites of Amino Acids. *J. Phys. Chem. Lett.* **2020**, *11*, 4346−4352.
(31) Cao, W.; Zhang, H.; Yuan, Q.; Zhou, X.; Kass, S. R.; Wang, X.-B. Observation of Conformational Simplification upon N-Methylation on Amino Acid Iodide Clusters. *J. Phys. Chem. Lett.* **2021**, *12*, 2780−2787.
(32) Hou, G.-L.; Wang, X.-B. Spectroscopic Signature of Proton Location in Proton Bound $HSO_4^-{\cdot}\ H^+{\cdot}\ X^-$ (X= F, Cl, Br, and I) Clusters. *J. Phys. Chem. Lett.* **2019**, *10*, 6714−6719.
(33) Wang, L.; Yuan, Q.; Cao, W.; Han, J.; Zhou, X.; Liu, S.; Wang, X.-B. Probing Orientation-Specific Charge-Dipole Interactions between Hexafluoroisopropanol and Halides: A Joint Photoelectron Spectroscopy and Theoretical Study. *J. Phys. Chem. A* **2020**, *124*, 2036−2045.
(34) Zhang, H.; Cao, W.; Yuan, Q.; Wang, L.; Zhou, X.; Liu, S.; Wang, X.-B. Spectroscopic Evidence for Intact Carbonic Acid Stabilized by Halide Anions in the Gas Phase. *Phys. Chem. Chem. Phys.* **2020**, *22*, 19459−19467.
(35) Hunter, E. P. L.; Lias, S. G. Evaluated Gas Phase Basicities and Proton Affinities of Molecules: An Update. *J. Phys. Chem. Ref. Data* **1998**, *27*, 413−656.
(36) Wyttenbach, T.; Witt, M.; Bowers, M. T. On the Stability of Amino Acid Zwitterions in the Gas Phase:The Influence of Derivatization, Proton Affinity, and Alkali Ion Addition. *J. Am. Chem. Soc.* **2000**, *122*, 3458−3464.
(37) Bush, M. F.; O'Brien, J. T.; Prell, J. S.; Saykally, R. J.; Williams, E. R. Infrared Spectroscopy of Cationized Arginine in the Gas Phase: Direct Evidence for the Transition from Nonzwitterionic to Zwitterionic Structure. *J. Am. Chem. Soc.* **2007**, *129*, 1612−1622.
(38) Milner, E. M.; Nix, M. G. D.; Dessent, C. E. H. Collision-Induced Dissociation of Halide Ion−Arginine Complexes: Evidence for Anion-Induced Zwitterion Formation in Gas-Phase Arginine. *J. Phys. Chem. A* **2012**, *116*, 801−809.
(39) Yuan, D.-F.; Liu, Y.; Qian, C.-H.; Zhang, Y.-R.; Rubenstein, B. M.; Wang, L.-S. Observation of a π-Type Dipole-Bound State in Molecular Anions. *Phys. Rev. Lett.* **2020**, *125*, 073003.
(40) Lu, Y.; Tang, R.; Ning, C. Observation of an Excited Dipole-Bound State in a Diatomic Anion. *J. Phys. Chem. Lett.* **2021**, *12*, 5897−5902.

https://doi.org/10.1021/acs.jpclett.1c03309
J. Phys. Chem. Lett. 2021, 12, 11022−11028

(41) Czekner, J.; Cheung, L. F.; Kocheril, G. S.; Wang, L.-S. Probing the Coupling of a Dipole-Bound Electron with a Molecular Core. *Chem. Sci.* **2019**, *10*, 1386−1391.
(42) Yuan, Q.; Cao, W.; Wang, X.-B. Cryogenic and Temperature-Dependent Photoelectron Spectroscopy of Metal Complexes. *Int. Rev. Phys. Chem.* **2020**, *39*, 83−108.
(43) Hanstorp, D.; Gustafsson, M. Determination of the Electron Affinity of Iodine. *J. Phys. B: At., Mol. Opt. Phys.* **1992**, *25*, 1773.
(44) Wang, X.-B.; Wang, L.-S. Photodetachment of Free Hexahalogenometallate Doubly Charged Anions in the Gas Phase: $[ML_6]^{2-}$, (M = Re, Os, Ir, Pt; L = Cl and Br). *J. Chem. Phys.* **1999**, *111*, 4497−4509.
(45) Wang, X.-B.; Wang, Y.-L.; Yang, J.; Xing, X.-P.; Li, J.; Wang, L.-S. Evidence of Significant Covalent Bonding in $Au(CN)_2^-$. *J. Am. Chem. Soc.* **2009**, *131*, 16368−16370.
(46) Dewar, M. J.; Zoebisch, E. G.; Healy, E. F.; Stewart, J. J. Development and Use of Quantum Mechanical Molecular Models. 76. AM1: A New General Purpose Quantum Mechanical Molecular Model. *J. Am. Chem. Soc.* **1985**, *107*, 3902−3909.
(47) Stewart, J. J. Optimization of Parameters for Semiempirical Methods II. Applications. *J. Comput. Chem.* **1989**, *10*, 221−264.
(48) *Spartan '08 for Macintosh*; Wavefunction, Inc.: Irvine, CA, 2008.
(49) Zhao, Y.; Truhlar, D. G. The M06 Suite of Density Functionals for Main Group Thermochemistry, Thermochemical Kinetics, Noncovalent Interactions, Excited States, and Transition Elements: Two New Functionals and Systematic Testing of Four M06-Class Functionals and 12 Other Functionals. *Theor. Chem. Acc.* **2008**, *120*, 215−241.
(50) Grimme, S.; Antony, J.; Ehrlich, S.; Krieg, H. A Consistent and Accurate ab Initio Parametrization of Density Functional Dispersion Correction (DFT-D) for the 94 Elements H-Pu. *J. Chem. Phys.* **2010**, *132*, 154104.
(51) Dunning, T. H., Jr Gaussian Basis Sets for Use in Correlated Molecular Calculations. I. The Atoms Boron Through Neon and Hydrogen. *J. Chem. Phys.* **1989**, *90*, 1007−1023.
(52) Papajak, E.; Zheng, J.; Xu, X.; Leverentz, H. R.; Truhlar, D. G. Perspectives on Basis Sets Beautiful: Seasonal Plantings of Diffuse Basis Functions. *J. Chem. Theory Comput.* **2011**, *7*, 3027−3034.
(53) Peterson, K. A.; Shepler, B. C.; Figgen, D.; Stoll, H. On the Spectroscopic and Thermochemical Properties of ClO, BrO, IO, and Their Anions. *J. Phys. Chem. A* **2006**, *110*, 13877−13883.
(54) Pritchard, B. P.; Altarawy, D.; Didier, B.; Gibson, T. D.; Windus, T. L. New Basis Set Exchange: An Open, Up-to-Date Resource for the Molecular Sciences Community. *J. Chem. Inf. Model.* **2019**, *59*, 4814−4820.
(55) Purvis, G. D., III; Bartlett, R. J. A Full Coupled-Cluster Singles and Doubles Model: The Inclusion of Disconnected Triples. *J. Chem. Phys.* **1982**, *76*, 1910−1918.
(56) Raghavachari, K.; Trucks, G. W.; Pople, J. A.; Head-Gordon, M. A Fifth-Order Perturbation Comparison of Electron Correlation Theories. *Chem. Phys. Lett.* **1989**, *157*, 479−483.
(57) Riplinger, C.; Pinski, P.; Becker, U.; Valeev, E. F.; Neese, F. Sparse Maps—A Systematic Infrastructure for Reduced-Scaling Electronic Structure Methods. II. Linear Scaling Domain Based Pair Natural Orbital Coupled Cluster Theory. *J. Chem. Phys.* **2016**, *144*, 024109.
(58) Weigend, F.; Köhn, A.; Hättig, C. Efficient Use of the Correlation Consistent Basis Sets in Resolution of the Identity MP2 Calculations. *J. Chem. Phys.* **2002**, *116*, 3175−3183.
(59) Frisch, M. J.; Trucks, G. W.; Schlegel, H. B.; Scuseria, G. E.; Robb, M. A.; Cheeseman, J. R.; Scalmani, G.; Barone, V.; Petersson, G. A.; Nakatsuji, H.; et al. *Gaussian 16, Rev. A.03*; Gaussian, Inc.: Wallingford, CT, 2016.
(60) Werner, H.-J.; Knowles, P. J.; Knizia, G.; Manby, F. R.; Schütz, M.; Celani, P.; Györffy, W.; Kats, D.; Korona, T.; Lindh, R.; et al. *MOLPRO, Version 2019.2, A Package of ab initio Programs*, 2019. https://www.molpro.net (accessed May 6, 2020).
(61) Neese, F. The ORCA Program System. *Wiley Interdiscip. Rev.: Comput. Mol. Sci.* **2012**, *2*, 73−78.
(62) Mozhayskiy, V.; Krylov, A. *ezSpectrum, Version 3.0*. http://iopenshell.usc.edu/downloads/ (accessed December 10, 2015).

https://doi.org/10.1021/acs.jpclett.1c03309
J. Phys. Chem. Lett. 2021, 12, 11022−11028